Centrifuge modelling of small earth dams subjected to the combined effects of rainfall and earthquakes

Izumi, Akira
Sawada, Yutaka
Hori, Toshikazu
Maki, Riku

(Citation)
Soil Dynamics and Earthquake Engineering,151:106963

(Issue Date)
2021-10-14

(Resource Type)
journal article

(Version)
Accepted Manuscript

(URL)
https://hdl.handle.net/20.500.14094/0100480889

Centrifuge Modelling of Small Earth Dams Subjected to the Combined Effects of Rainfall and Earthquakes

Akira Izumi[1], Yutaka Sawada[2*], Toshikazu Hori[3], Riku Maki[4]

1 Institute for Rural Engineering, NARO, 3-1-1 Kannondai, Tsukuba, Ibaraki 305-8517, Japan
Email: izumia309@affrc.go.jp

2 Graduate School of Agricultural Science, Kobe University, Rokkodai-cho, Nada-ku, Kobe, Hyogo 657-8501, Japan
Email: sawa@harbor.kobe-u.ac.jp

3 Institute for Rural Engineering, NARO, 3-1-1 Kannondai, Tsukuba, Ibaraki 305-8517, Japan
Email: thori@affrc.go.jp

4 Institute for Rural Engineering, NARO, 3-1-1 Kannondai, Tsukuba, Ibaraki 305-8517, Japan
Email: makir514@affrc.go.jp

*Corresponding author: Yutaka Sawada

Abstract

In this study, the combined effects of rainfall and earthquakes on earth dams were modelled using a 1/40 scale model embankment, spraying device, and shaking table. Two scenarios were tested: one where the embankment was subjected to seismic motion after rainfall, and another where the embankment was subjected to rainfall after seismic motion. When the rain occurred first, causing the phreatic line to rise, the excess pore-water pressure at the toe of the embankment was higher than if there had been no rainfall, and the seismic stability of the embankment deteriorated. When the shaking occurred first, cracks due to seismic motion promoted subsequent rainfall seepage, increasing the amount of eroded soil in the embankment. Thus, rainfall damage and seismic damage influence and exacerbate each other.

KEYWORDS: Centrifuge modelling; Earth dams; Phreatic line; Rainfall damage; Seismic damage

1. Introduction

Small earth dams have long been built to secure agricultural water supplies in areas where groundwater or water from large rivers is not available. Although such old dams are less than 10 m high, they are often weak or unstable because they were built without modern construction techniques such as the use of compaction machines and the regulation of water content. Heavy rainfall and consequent flooding—which have increased rapidly worldwide in recent years because of rapid climate change—can damage them in several ways: e.g., the increased seepage pressure due to a rapid rise in water level can cause piping failure; flow overtopping can cause erosion failure of the embankment; and rainfall seepage to the downstream (non-reservoir) side of the dam can cause sliding and slope failure (Hori et al., 2002; Hori, 2005). Moreover, many small earth dams are located in earthquake-prone regions. Earthquakes usually cause longitudinal and cross-sectional cracks in the crown of the dam. Slope sliding and failure and the liquefaction of embankment foundations are also quite common (Moriya and Kawaguchi, 1970; Tani, 1996; Hasegawa and Murakami, 1996; Tani, 2000; Mohri et al., 2014).

In Asia, there are many reservoirs; the importance of maintenance enhancement at the dams has been highlighted by the large number of recent rainfall-related floods. Fujita (2009) reported a case of natural earth dams affected by a typhoon in Taiwan in 2009, and Salika et al. (2018) have discussed how, in Sri Lanka, proper maintenance of small earth dams against heavy rainfall can mitigate the danger of flood damage.

There are approximately 160,000 small earth dams in Japan. From 1999 to 2018, 7,435 were damaged by heavy rainfall, and 2,207 by earthquakes (Ministry of Agriculture, Forestry, and Fisheries, 2020). Thus, the combined effect of earthquakes and heavy rainfall on structures merits attention. Ren et al. (2020), studying the earthquake resistance of reinforced-soil retaining walls subjected to the combined effects of rainfall and earthquake, performed shaking-table tests with five different degrees of saturation of the model ground, and demonstrated that the wall displacement and reinforcement strain were larger under saturated than unsaturated conditions. Studies on the combined effects of earthquakes and heavy rainfall on structures have recently begun, and earth dams have not been considered, except in the small model experiments reported by Nakazawa et al. (2020). There is also no study yet on modelling the combined effects of rainfall and earthquakes using centrifuge tests.

There have been many studies on the behaviour of embankments and natural slopes during earthquakes; our attention is restricted to studies that are based on earth-dam-model experiments. One line of research has addressed the behaviour of earth dams during earthquakes in the case where there is no stored water. Shear strain in embankment bodies has been examined for this situation (Ohne et al., 1983), and the dams' basic vibration characteristics and failure status have been studied with shaking-table tests on small-scale

models (Hasegawa, Kikuchi, 1981).

Other researchers have considered the case where the reservoir is not empty. Torisu et al. (2011) reported that, when shaking-table tests in a gravitational field were carried out in the presence of stored water on an earth-dam model made of sand with a central core and an embankment height of 40 cm, the deformation of the embankment increased with decreasing density of the sand. Moreover, the deformation of the upstream side was larger than that of the downstream side. Takada et al. (2020) carried out shaking-table tests using a geotechnical centrifuge on an embankment model made of kaolin–sand soil mixture with a changing water-storage level; the saturated region in the embankment, subsidence at the crown, and embankment deformation were found to be larger when the water storage level was higher. Sawada et al. (2018) prepared large-scale embankments with inclined cores and heights of 3 m, using construction machinery to compact fine-grained soil of the kind actually utilised in small earth dams. In shaking-table tests, the deformation of such an embankment was larger on the upstream side. Negative pore-water pressure, an indicator of the undrained condition of the soil, was measured on the upstream side, indicating the importance of compacting.

To suppress rainfall seepage, Hori et al. (2013) proposed installing a thin layer as a coating on the surface of the embankment and verified the effects of suppressing rainfall seepage and erosion using rainfall, overtopping, and wave experiments. Rainfall simulators are being developed for use in centrifuge modelling (Bhattacherjee and Viswanadham, 2018; Khan et al., 2018; Zhang et al., 2011; Matziaris et al., 2015; Ling et al., 2014) to study seepage in embankments and slopes and the accompanying stability problems.

Tani et al. (1990) proposed reinforcement of embankments using continuous fibres and tested the earthquake resistance of their construction method using shaking-table tests with a 40 cm high earth-dam model. Mohri et al. (2009) proposed earth dams with embankment slopes reinforced using sandbags; the erosion resistance of such dams was studied using flow-overtopping tests, and their earthquake resistance using large-scale shaking-table tests. Momiyama et al. (2020) proposed a construction method utilising steel-sheet piles for the reinforcement of earthen embankments from the crown shoulder up to the foundation, and verified its earthquake resistance, water-shielding effect, and erosion resistance using model experiments.

As described above, many experimental studies have been conducted on the stability of earth dams in the event of an earthquake or rainfall seepage separately, and corresponding corrective measures have been proposed. However, there are hardly any studies on the *combined* effects of rainfall and earthquakes on earth dams. Two scenarios can be imagined: 1) an earthquake occurs after rainfall, and 2) rainfall occurs after an earthquake. In the first case, the prior rainfall may cause a rise in phreatic lines and in saturation

of the embankment (especially the downstream slope), affecting the stability under subsequent seismic motions. In the second case, rainfall permeates the cracks in the embankment caused by seismic motion, inducing erosion. In this study, centrifuge modelling tests were conducted for both scenarios.

2. Test overview

2.1 Test setup

A schematic overview of the system used for centrifuge modelling of the combined effects of rainfall and earthquakes is shown in Fig. 1.

2.1.1 Centrifuge test equipment

A beam-type centrifuge at the Institute of Rural Engineering, NARO, was used for the tests. The length of the arm was 4.8 m. Table 1 provides the specifications of the test equipment, with which it was possible to subject the model to accelerations of up to 100 G. The equipment included a one-dimensional shaking table.

2.1.2 Soil container

An aluminium container with internal dimensions of 1,000 mm width, 300 mm depth, and 500 mm height was used in the tests. The front end of the soil container was made of tempered glass to enable observation of the status before and after the tests. At 50 mm from both ends, partition plates were installed for water supply and drainage. A rain gutter was installed on the wall at a position higher than the embankment height to prevent rainwater from flowing along the wall surface.

During shaking, the reflected waves from the container affect the dam model. In shaking-table tests for reinforced retaining walls, EPS (expanded polystyrene) blocks are placed at the boundary between the container and the model retaining wall to absorb the reflection of the waves within the model due to induced seismic excitation (e.g., Kilic et al., 2021). As only the foundation was in contact with the wall of the container in this study, the effect on the main body of the dam was considered to be relatively small; thus, no countermeasure such as EPS was applied.

2.1.3 Rainfall simulator

The rainfall simulator is shown in Fig. 1. It consisted of eight nozzles capable of spraying pressurised air and pressurised water, two steel pipes for water supply, and one steel pipe for air supply. To reduce the effects of the Coriolis force, the nozzles were placed at a constant height from the slope surface. A lid was

installed at the top of the soil container to prevent the scattering of rain droplets outside.

To obtain a clear understanding of rainfall distribution, preliminary tests were conducted on a Styrofoam embankment model fitted with a cubic measuring cup 57 mm long on each side. It was established that 25 mm/h of rainfall could be achieved when the model was subjected to a centrifugal acceleration of 40 G.

2.1.4 Device for sustaining constant water level

The level of stored water in the reservoir was regulated using the device shown in Fig. 2, which could maintain any arbitrary water level using a motor.

2.2 Model materials

The dam model in this study had a sloping core. Sandy soil from Ibaraki prefecture was used as the core material. Sandy soil from Gunma prefecture was used as the embankment material and foundation. The coefficients of permeability for the core material and the embankment material were 5.73×10^{-7} m/s and 2.83×10^{-7} m/s, respectively. Fig. 3 shows the grain-size cumulative curves, and Fig. 4 shows the compaction curves. Table 2 shows the physical properties of the materials.

In centrifuge tests, it is common to represent water by a viscous fluid, such as Metolose, to satisfy Darcy's law. However, Metolose would clog the sprayer of the rainfall device; hence, water was employed instead. When water is used in the 40 G centrifugal-acceleration field of this study, the hydraulic gradient (and therefore the seepage velocity) is 40 times larger than that of the prototype. This means that the hydraulic conductivities of the above core and embankment materials correspond to 2.29×10^{-5} m/s and 1.13×10^{-5} m/s, respectively. These permeabilities are large for retrofitted dams but exist in deteriorated dams.

2.3 Model construction

An embankment model, shown in Fig. 5, was built for the tests. The thickness of the foundation was 100 mm, the height of the embankment was 200 mm with a crown width of 75 mm, and the upstream and downstream slopes had a 1:1.5 gradient. This model was subjected to a centrifugal acceleration of 40 G, making it equivalent to an embankment of height 8 m and crown width 3 m under 1 G conditions. Both the foundation and the embankment body were compacted by 20 mm per layer to achieve 95% of the maximum dry density based on the Proctor compaction test. The stored-water level was 130 mm from the base, equivalent to 5.2 m under 1 G conditions.

2.4 Measuring devices

For the tests, accelerometers and pore-water pressure-gauges were installed inside the embankment, as shown in Fig. 5. The magnitude of subsidence of the embankment when subjected to shaking cannot be measured using a laser displacement meter (LDM) because of the effects of rainfall. Accordingly, after subjecting the model to shaking and rainfall, the centrifuge was stopped, the rainfall simulator device was detached, and the deformation of the embankment in the longitudinal direction was measured at intervals of 5 cm from the soil-container wall using the LDM.

2.5 Test cases and conditions

The embankment model was installed on the centrifuge platform and subjected to 40 G centrifugal acceleration. Water was then poured from the constant-water-level-sustaining device. The tests for each case were conducted once the water level reached 130 mm, after confirming (by measuring the pore-water pressure) that equilibrium (steady state) had been achieved.

Table 3 lists the test conditions. In Case 1, the embankment model was subjected to 25 mm/h rainfall and then to sinusoidal shaking with amplitude 3.0 m/s^2 at 5 Hz. Rainfall was applied for 15 min till the phreatic line inside the embankment became steady. Although the duration was long considering the actual time, it was determined as the time till deformation caused by erosion became steady. The interval between the rainfall and earthquake was determined as approximately 1 min, which was equivalent to 1 day of the actual time. Regarding the shaking, the tapered part was 2 s long. The duration of the target acceleration was 60 s (i.e., 300 waves). Fig. 6 shows the acceleration waveform equivalent to that of 1 G conditions.

In Case 2, the order was reversed: the embankment model was subjected to sinusoidal shaking with amplitude 3.0 m/s^2 at 5 Hz and then to 25 mm/h of rainfall. In Case 3, the embankment model was subjected to two sinusoidal shakings at 5 Hz, the first with amplitude 3.0 m/s^2 and the second 5.0 m/s^2, and then to rainfall of 25 mm/h.

The effect on stability against seismic motion of the rise in phreatic lines and increased saturation in the embankment due to prior rainfall was elucidated by comparing the results in Cases 1 and 2. The effect of rainfall on slope erosion caused by cracks or sliding failure occurring in the embankment due to prior seismic motion was elucidated by comparing the results after rainfall in Case 1 to those in Cases 2 and 3.

3. Results and discussion

3.1 Effect of prior rainfall on dynamic behaviour of embankment during earthquake (Scenario I)

In this section, the effect of prior rainfall on the earthquake resistance of the embankment is described by comparing the results of Case 1, where the embankment was subjected to rainfall prior to shaking, to

the intermediate results of Case 2, where the embankment was subjected to shaking without any rainfall. Note that the values given in the discussion are converted to 1 G fields (gravitational fields).

3.1.1 Differences in phreatic line with and without rainfall

To study the effect of prior rainfall on the earthquake resistance of an embankment, it is necessary to identify the location of the phreatic line within the embankment body with and without rainfall. In this study, the location of the phreatic line was estimated based on readings from the pore-water pressure-gauges installed within the embankment body. Fig. 7 shows the estimated phreatic lines. As can be seen in Fig. 7, the phreatic line in Case 1 was elevated because of prior rainfall. The elevation was maximal near the middle of the embankment, and the elevation in water level compared to the steady state was 0.76 m. However, during the few minutes after the end of prior rainfall before the embankment was subjected to shaking, the phreatic-line elevation dropped; at the start of shaking, the water level near the middle of the embankment was only 0.32 m above the steady-state value. By contrast, in Case 2, where the embankment was not subjected to prior rainfall, the phreatic line in the middle of the embankment was located before shaking at a height of 6.68 m from the soil container bottom. This was 0.72 m lower than the position of the corresponding phreatic-line water level (7.4 m) at the time of the start of shaking in Case 1, clearly indicating the difference in phreatic lines between Cases 1 and 2.

3.1.2 Effect of prior rainfall on deformation of embankment

This subsection describes the difference in the after-shaking embankment shape because of prior rainfall. Fig. 8 shows the state of the embankment, as observed from the front end of the soil container, for Cases 1 and 2 after shaking. Although sliding failure was observable at a height of approximately 1.2 m near the toe of the embankment on the downstream side in Case 1, no such sliding failure occurred in Case 2.

Fig. 9 shows the results of LDM measurements of the embankment shape after shaking for Cases 1 and 2. The magnitude of deformation near the embankment toe on the downstream side was greater for Case 1. The position of this deformation roughly agrees with the position of the sliding observed in Fig. 8.

Fig. 10 shows the time history of the excess pore-water-pressure ratio calculated from the readings of pore-water pressure-gauge P4, installed near the embankment toe on the downstream side. As can be seen in Fig. 10, although the pore-water-pressure ratio at P4 increased to 0.6 in Case 1, the increase in Case 2 was quite small: only about 0.16. These results demonstrate that, as the prior rainfall increased the magnitude of deformation near the toe of the embankment on the downstream side and thereby expanded the saturated area, the strength of the embankment soil decreased. For the embankment subjected to prior rainfall, the phreatic line was elevated above that in the steady state, clearly indicating a high risk of sliding

at the toe of the embankment on the downstream side.

3.2 Effect of rainfall after earthquake on erosion of embankment (Scenario II)

This section describes the effect of rainfall occurring after an earthquake on the shape deformation of an embankment, based on the results from Case 1, where the embankment was first subjected to rainfall, and Case 2, where the embankment was first shaken. Moreover, to investigate how the effect of rainfall depends on differences in the prior damage status of the embankment, the results for Case 2 are compared with those for Case 3, where the shaking acceleration was increased.

3.2.1 Elevation of phreatic line due to rainfall after earthquake

As in Section 3.1, the changes in the phreatic-line position caused by rainfall and earthquakes are compared to the steady state of the internal embankment body. Fig. 11 shows the position of the phreatic lines as estimated from the pore-water pressure-gauge readings after the embankment was subjected to rainfall in Cases 1–3. At both the start and end of rainfall, the phreatic-line position was highest in Case 3. Fig. 12 shows the sloping-core status after completion of the tests in Cases 2 and 3. The sloping core was more severely damaged in Case 3, where an approximately 5.0 m/s^2 shaking was applied after a shaking of 3.0 m/s^2, than in Case 2, where only the first shaking was applied. These results indicate that, in Case 3, the phreatic line was elevated because adequate water-shielding performance could not be realised.

3.2.2 Elevation of erosion volume due to rainfall after earthquake

This subsection describes the effect of rainfall after shaking on deformation by comparing the shape of the embankment in Cases 1–3. Note that, for Case 1, LDM measurements of the embankment were not performed after rainfall because the model was subjected to shaking immediately after being subjected to rainfall. Accordingly, for Case 1, the discussion is based only on the images captured during the tests.

Fig. 13 shows the status of the embankment before and after it was subjected to rainfall in Case 1; it can be seen that there was no change in the embankment shape. Fig. 14 shows the results of the LDM measurements for Cases 2 and 3. (Note that the measurement results shown here correspond to a position 20 cm from the front end of the soil container.) For Case 2, there was almost no change in the shape of the slope on the upstream side after shaking and rainfall, but on the downstream side the deformation generated by shaking was exacerbated by the rainfall that followed. It is likely that this was because the shaking caused minute damage to the downstream-slope surface of the embankment, and the surface soil at these damaged points was washed away by the subsequent rainfall. Similarly, in Case 3, although there was no significant change in the shape of the upstream-slope surface after the shaking and rainfall, the

deformation of the downstream slope caused by the shaking was increased by the subsequent rainfall. Based on the results shown in Figs. 13 and 14, even rainfall not sufficient to cause any change in an undamaged embankment can have large effects on an embankment damaged by a prior earthquake.

Next, the status of the embankment in Cases 2 and 3 clarifies the factors that increase embankment deformation due to rainfall after shaking. Fig. 15 shows the status of the downstream-slope surface before and after rainfall in Cases 2 and 3. In both cases, several cracks appeared after shaking; subsequent rainfall caused the deformation near these cracks to progress. These results suggest that rainwater seeped into cracks produced by shaking, and the consequent soil-particle runoff near these cracks worsened the deformation. As shown in Fig. 14, for Case 3, where damage due to shaking was larger than that in Case 2, the extent of deformation due to rainfall after shaking was also larger. This indicates that the size of the cracks generated by shaking correlates with the progress in embankment deformation because of rainfall seepage.

Next, for Cases 2 and 3, the effect of rainfall after shaking on the extent of embankment deformation was evaluated using LDM measurements of the embankment shape. The LDM was used to measure the shape of the embankment at five positions at distances of 5, 10, 15, 20, and 25 cm from the front end of the soil container. Using the shape measurements at two adjacent cross-sections, the average extent of deformation after erosion from the initial state was calculated. By multiplying this value by the distance of 5 cm between the measurement positions, the volume of erosion was calculated at each measurement position. The extent of deformation due to embankment erosion was calculated by summing the erosion volumes at all measurement positions. The result in Case 2 was 1,098.1 cm^3; that in Case 3 was 4,492.7 cm^3. Thus, the extent of deformation in Case 3 was approximately four times that in Case 2. This observation demonstrates that, in Case 3, where the level of shaking was stronger, the embankment damage was significant, and that rain-induced soil runoff occurred at the damaged area downstream, considerably reducing the stability of the embankment.

3.3 Magnitude of damage by earthquake loading

In this section, the magnitude of damage to the embankment in the present study is compared with that of the actual embankments. Swaisgood (2003) analysed approximately 70 case histories of various types of dam embankments that had experienced earthquake. It is stated in the paper that the crest settlement ratio of the embankment is closely related to the maximum ground acceleration and the magnitude of damage. The crest settlement ratio *CS* is given by the following equation.

$$CS = \frac{\Delta h}{DH + AT} \times 100,$$

where Δh is the settlement of crest, *DH* is the height of the dam, and *AT* is the depth of the ground.

Fig. 16 shows the relations between peak ground accelerations and crest settlement ratios. The settlement ratios of Case 1 and Case 2 are classified as moderate. Even though the peak acceleration in Case 1 is smaller than that in Case 2, the settlement ratio in Case 1 is slightly larger than that in Case 2. In Case 1, sliding failure occurred at a height of approximately 1.2 m near the toe of the embankment on the downstream side as shown in Figs. 8(a) and 9(a). In Case 2, several cracks appeared as shown in Fig. 15(a); however, the total damage was smaller than that in Case 1. Regarding Case 3, the damage is classified as serious. In Case 3, many cracks appeared, and the embankment deformed at both sides as shown in Figs. 14(b) and 15(c). Overall, the damage in this study appears to be somewhat greater than the damage in the field. This can be attributed to the fact that the excitation in this study was sinusoidal, and large accelerations close to the peak acceleration were repeated.

4. Conclusion

In this study, centrifuge-model tests targeting reservoirs with an 8 m high embankment were conducted to elucidate the dynamic behaviour of reservoirs under disastrous combinations of rainfall and earthquakes. The findings are as follows:

The target rainfall level was achieved using a centrifuge-model rainfall simulator with nozzles placed at certain distances from the embankment-slope surface to spray pressurised water and air. A shaking table was used to simulate earthquake conditions.

It was observed that, in the event of an earthquake occurring after rainfall, there was no significant effect on the embankment shape deformation on the upstream side. However, sliding failure occurred on the downstream side of the embankment because of the elevation of the phreatic line after rainfall.

It was also observed that even rainfall insufficient to cause any change in the shape of the embankment in the absence of seismic motion can significantly affect the progress of earthquake-induced deformations. Moreover, the progress of deformation was more prominent near cracks. This is evidence that seismic damage makes the soil prone to rainfall seepage. Additionally, an increase in the magnitude of seismic motion significantly increased the amount of soil erosion due to rainfall and reduced the stability of the embankment.

The above findings demonstrate that the occurrence of a previous disaster will influence the effects of a later one.

Funding

This work was supported by JSPS KAKENHI Grant Number 18H02298.

References

ASTM (2006) Standard Practice for Classification of Soils for Engineering Purpose (Unified Soil Classification System), D2487-06.

Bhattacherjee, D. and Viswanadham, B.V.S. (2018) Development of a rainfall simulator in centrifuge using Modified Mariotte's principle, *9th International Conference on Physical Modelling in Geotechnics*, pp. 337-342.

Fujita, M. (2009) Sediment disasters and flood disasters in Taiwan triggered by Typhoon Morakot 2009, *Disaster Prevention Research Institute Annuals*, Vol. 53, pp. 73-83. (in Japanese)

Hasegawa, T. and Kikusawa, M. (1981) The behaviour of a fill-type dam model under dynamic loading by shake table-dynamic characteristics of fill-type dams(I), *Transactions of The Japanese Society of Irrigation, Drainage and Reclamation Engineering*, Vol. 95, pp. 57-64. (in Japanese)

Hasegawa, T. and Murakami, A. (1996) Damage to agricultural facilities, *Soils and Foundations*, Vol. 36, pp. 255-261.

Hori, T., Mohri, Y. and Aoyama, S. (2002) Causes and features of damage to small earth dams induced by heavy rainfall, *Transactions of The Japanese Society of Irrigation, Drainage and Rural Engineering*, No. 218, pp. 127-137. (in Japanese)

Hori, T. (2005) Damages of small earth dams for irrigation induced by heavy rainfall, *Bulletin of the National Research Institute of Agricultural Engineering*, Vol. 44, pp. 139-247. (in Japanese)

Khan, I.U., Al-Fergani, M. and Black, J.A., (2018) Development of a rainfall simulator for climate modelling, *9th International Conference on Physical Modelling in Geotechnics*, pp. 507-512.

Kilic, I.E., Cengiz, C., Edincliler, A. and Guler, E. (2021) Seismic behavior of geosynthetic-reinforced retaining walls backfilled with cohesive soil, *Geotextiles and Geomembranes*, DOI: 10.1016/j.geotexmem.2021.04.004

Ling, H.I., Wu, M.-H., Leshchinsky, D. and Leshchinsky, B. (2009) Centrifuge modeling of slope instability, *Journal of Geotechnical and Geoenvironmental Engineering*, Vol. 135, pp. 758-767.

Matziaris, V., Marshall, A.M. and Yu, H.-S. (2015) *Recent Advances in Modeling Landslides and Debris Flows*, pp. 73-83. Springer, Cham.

Ministry of Agriculture, Forestry and Fisheries [of Japan], (2020) Disaster mitigation of small earth dam. https://www.maff.go.jp/j/nousin/bousai/bousai_saigai/b_tameike/attach/pdf/index-68.pdf, accessed 26/03/2021 (In Japanese).

Mohri, Y., Masukawa, S., Hori, T. and Ariyoshi, M. (2014) Damage to agricultural facilities, *Soils and Foundations*, Vol. 54, No. 4, pp. 588-607.

Mohri, Y., Matsushima, K., Yamazaki, S., Lohani, T.N., Tatsuoka, F. and Tanaka, T. (2009) New direction for earth reinforcement: disaster prevention for earthfill dams, *Geosynthetics International*, Vol. 16, No. 4, pp. 246–273.

Momiyama, T., Taenaka, S., Hara, T. and Tanaya, N. (2020) Study on reinforcement method of small earth dams using steel sheet piles: Verification of reinforcement effect against the liquefaction through the shaking test, *Transactions of The Japanese Society of Irrigation, Drainage and Rural Engineering*, Vol. 88, No. 1, pp. I47-I58.

Moriya, M. and Kawaguchi, N. (1970) Damage to small earthfill irrigation dams in Aomori prefecture during the Tokachioki earthquake, *Soils and Foundations*, Vol. 10, No. 2, pp. 72-82.

Nakazawa, H., Ishizawa, T., Danjo, T., Sawada, Y. and Onoue, Y. (2020) Model tests on the deformation and collapse processes of small earth dams due to earthquakes and rainfall, *Proceedings of the 17th World Conference on Earthquake Engineering,* 4c-0026.

Ohne, Y., Tatebe, K., Narita, K. and Okumura, T. (1983) Fundamental study on earthquake resistant design of fill-type dams, *Transactions of the Japan Society of Civil Engineers*, Vol. 339, pp. 127-136. (in Japanese)

Ren, F., Huang, Q. and Wang, G. (2020) Shaking table tests on reinforced soil retaining walls subjected to the combined effects of rainfall and earthquakes, *Engineering Geology*, Vol. 267, p. 105475.

Salika T., Nimal W. and Lalith, R. (2018) Holistic behavior of urban pond systems for flood risk mitigation – A case study in Jaffna Municipal Council Area, *International Conference on Sustainable Built Environment.*

Sawada, Y., Nakazawa, H., Oda, T., Kobayashi, S., Shibuya, S. and Kawabata, T. (2018) Seismic performance of small earth dams with sloping core zones and geosynthetic clay liners using full-scale shaking table tests. *Soils and Foundations*, Vol. 58, No. 3, pp. 519-533.

Swaisgood, J.R., (2003) Embankment dam deformations caused by earthquakes, *In: Pacific Conference on Earthquake Engineering*, Paper no. 014.

Takada, Y., Ueda, K. and Uzuoka, R. (2020) Seepage-seismic coupled behaviour of small scale earth dams considering countermeasure techniques, *Journal of Japan Society of Civil Engineers, Ser. C (Geosphere Engineering)*, Vol. 76, No. 3, pp. 254-265. (in Japanese)

Tani, S. (1996) Damage to earth dams, *Soils and Foundations*, Vol. 36, pp. 263-272.

Tani, S. (2000) Behavior of large fill dams during earthquake and earthquake damage, *Soil Dynamics and Earthquake Engineering*, Vol. 20, pp. 223-229.

Tani, S., Yamashita, T., Nakayama, K., Ishizaki, H. and Takano, Y. (1990) Reinforcement of embankment by continuous fibers, *Journal of JSIDRE*, Vol. 58, No. 9, pp. 869-874.

Torisu, S.S., Sato, J., Towhata, I., and Honda, T. (2010) 1-G model tests and hollow cylindrical torsional shear experiments on seismic residual displacements of fill dams from the viewpoint of seismic performance-based design, *Soil Dynamics and Earthquake Engineering*, Vol. 30, No. 6, pp. 423-437.

Zhang, G., Qian, J.-Y., Wang, R. and Zhang, J.-M. (2011) Centrifuge model test study of rainfall-induced deformation of cohesive soil slope, *Soils and Foundations*, Vol. 51, No. 2, pp. 297-305.

Table 1 Specification of the centrifuge test equipment

Platform	Length	2,400 mm
	Width	1,600 mm
	Height	1,000 mm
Maximum Centrifuge Force	Static Test	100 G
	Dynamic Test	75 G
Maximum Loading Weight		3 tf
Maximum Rotating Speed		137 rpm

Table 2 Physical properties of embankment and core materials

	Embankment material	Core material
Soil particle density ρ_s (g/cm^3)	2.704	2.592
Average diameter D_{50} (mm)	0.347	0.331
Uniformity coefficient U_C	121	305
Coefficient of curvature U_C'	9.7	10.4
Liquid limit W_L (%)	23.7	45.5
Plastic limit W_P (%)	NP	35.7
Plasticity index I_P	NP	9.9
Classification by ASTM (2006)	SM	SM

Table 3 Test cases

Case	Test conditions
Case 1	Rainfall→Shaking
Case 2	Shaking→Rainfall
Case 3	Shaking twice→ Rainfall

FIGURE CAPTIONS:

Fig. 1. Schematic diagram of test setup. Dam model with shaking device and eight-nozzle rainfall simulator are spun in a centrifuge to simulate gravity.

Fig. 2. Schematic illustration of device for sustaining constant water level on side of dam model opposite rainfall simulator.

Fig. 3. Grain-size cumulative curves for embankment and core materials used in dam model.

Fig. 4. Compaction curves for embankment and core materials used in dam model.

Fig. 5. Cross-sectional diagram of embankment.

Fig. 6. Shaking-table acceleration history: (a) first shaking; (b) second shaking.

Fig. 7. Phreatic line: (a) Case 1 (rainfall, then shaking); (b) Case 2 (shaking only) before shaking, with Case 1 curve for comparison.

Fig. 8. Status of downstream embankment slope after shaking: (a) Case 1 (rainfall, then shaking); (b) Case 2 (shaking only). Red circle in (a) indicates sliding failure.

Fig. 9. Embankment shape after shaking: (a) Case 1 (rainfall, then shaking); (b) Case 2 (shaking only).

Fig. 10. Excess pore-water-pressure ratio at the toe of the embankment on the downstream side. (Case 1, rainfall, then shaking; Case 2, shaking only.)

Fig. 11. Phreatic line before and after rainfall: (a) Case 1 (rainfall only); (b) Case 2 (moderate shaking, then rainfall); (c) Case 3 (moderate shaking, then severe shaking, then rainfall).

Fig. 12. Status of water-shielding zone (sloping core) after tests: (a) Case 2 (one shaking); (b) Case 3 (two increasingly severe shakings).

Fig. 13. Embankment status (a) before and (b) after rainfall in Case 1 (rain, then shaking). There was almost no deformation.

Fig. 14. Embankment status after completion of tests in (a) Case 2 (one shaking, then rain) and (b) Case 3 (two increasingly severe shakings, then rain). Although rainfall does not normally deform an undamaged embankment, it causes erosion when rainfall seepage occurs in cracks generated by shaking.

Fig. 15. Status of damage to downstream-slope surface after (left) shaking and (right) rainfall in (top) Case 2 (one shaking before rain) and (bottom) Case 3 (two shakings before rain).

Fig. 16. Relations between peak ground accelerations and crest settlement ratios (modified from Swaisgood, 2003).

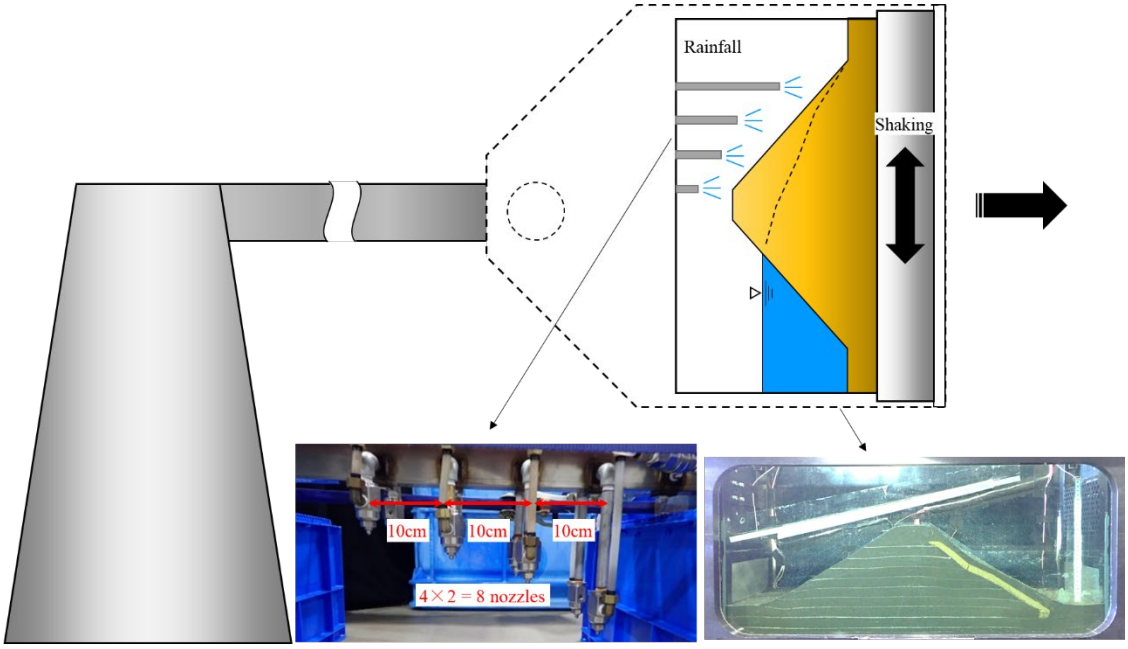

Fig. 1. Schematic diagram of test setup. Dam model with shaking device and eight-nozzle rainfall simulator are spun in a centrifuge to simulate gravity.

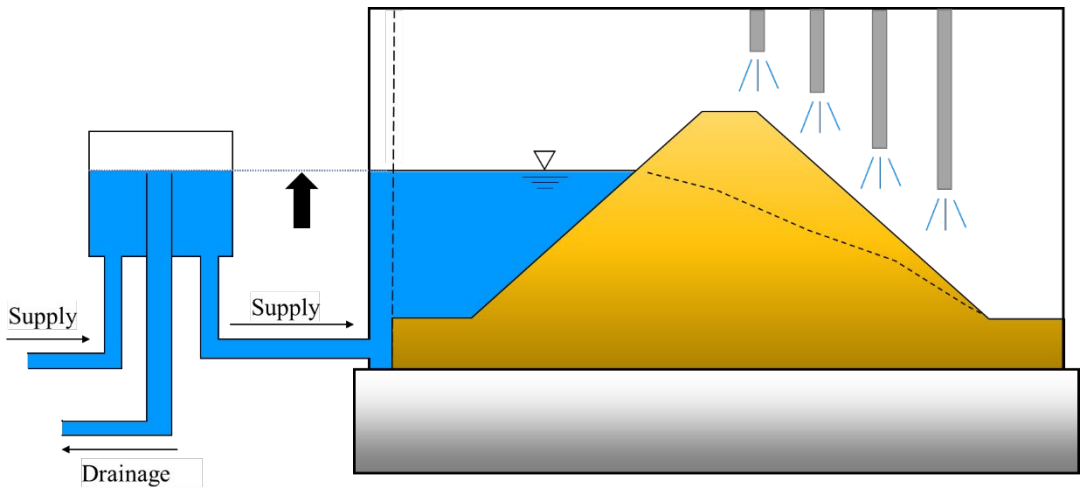

Fig. 2. Schematic illustration of device for sustaining constant water level on side of dam model opposite rainfall simulator.

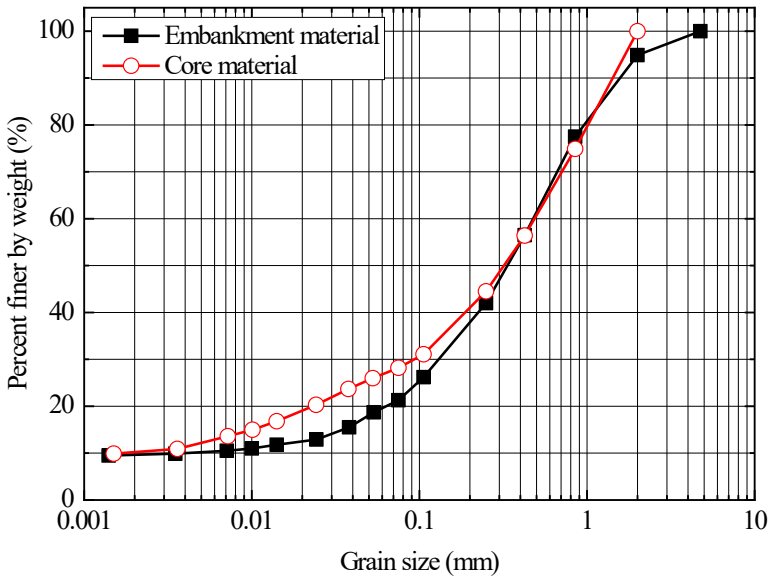

Fig. 3. Grain-size cumulative curves for embankment and core materials used in dam model.

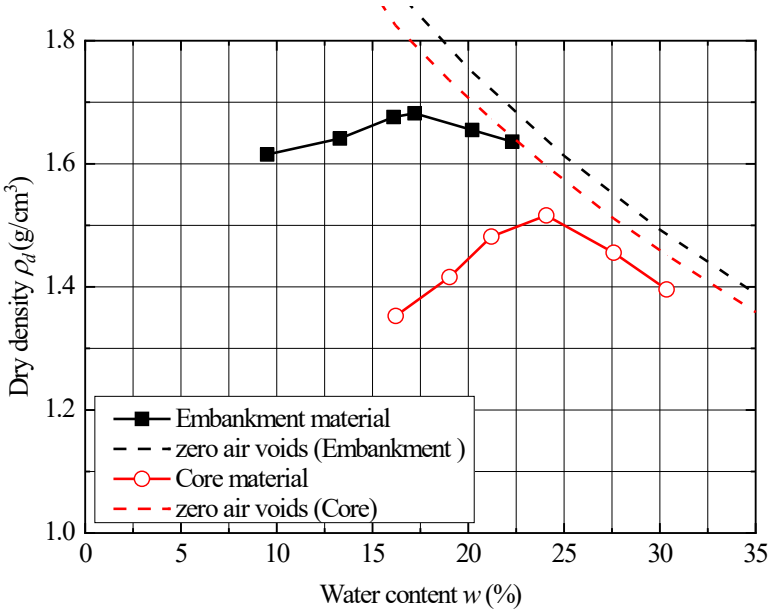

Fig. 4. Compaction curves for embankment and core materials used in dam model.

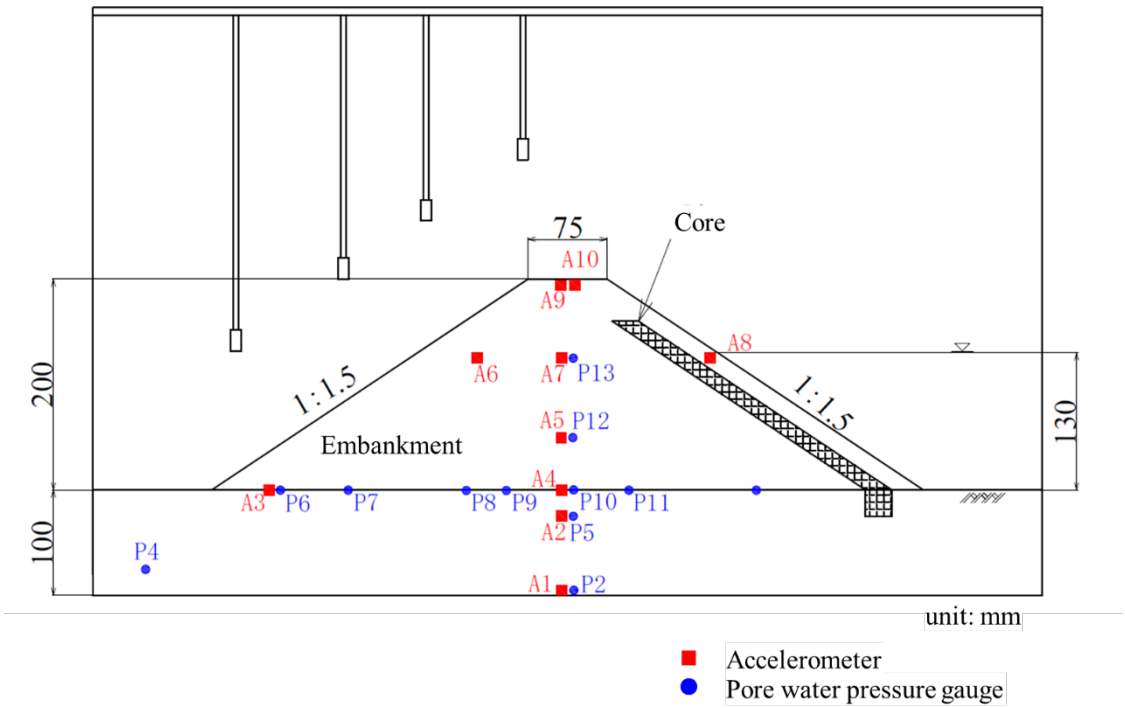

Fig. 5. Cross-sectional diagram of embankment.

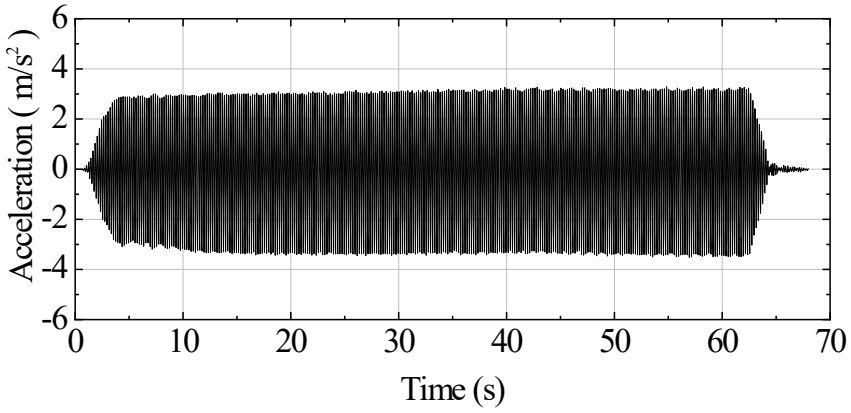

(a)

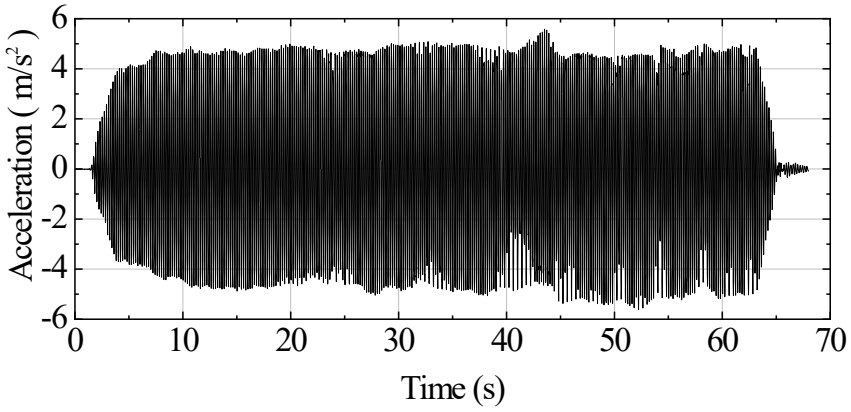

(b)

Fig. 6. Shaking-table acceleration history: (a) first shaking; (b) second shaking.

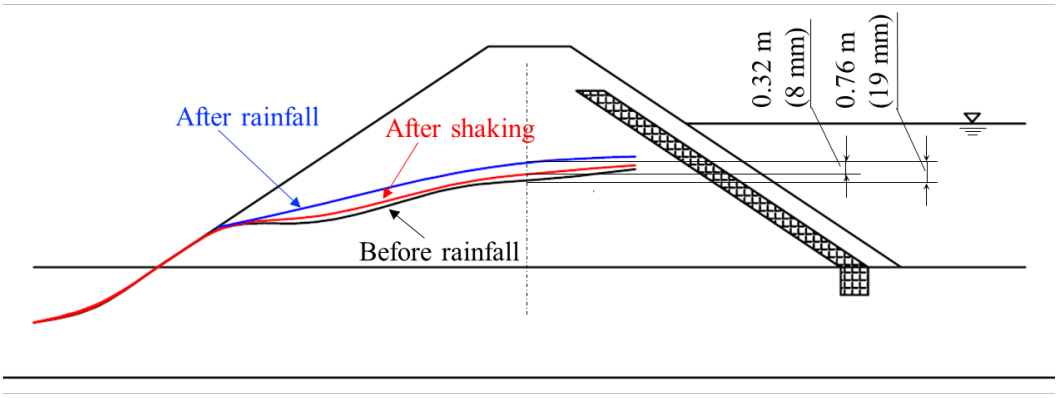

(a)

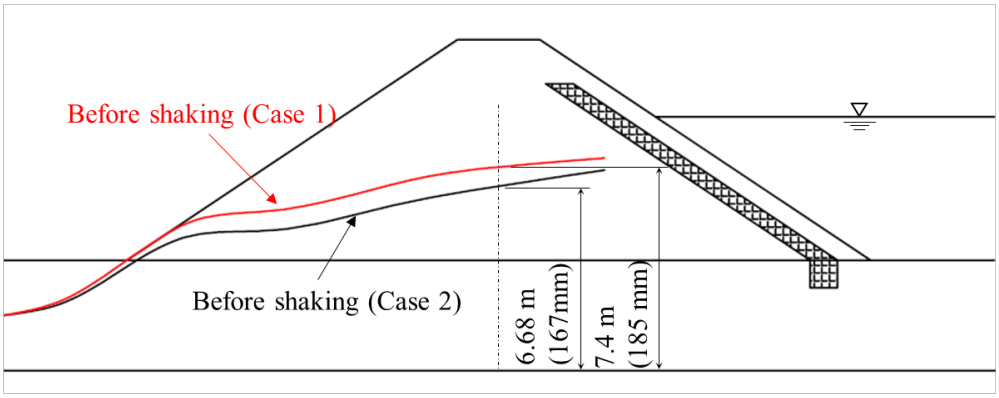

(b)

Fig. 7. Phreatic line: (a) Case 1 (rainfall, then shaking); (b) Case 2 (shaking only) before shaking, with Case 1 curve for comparison.

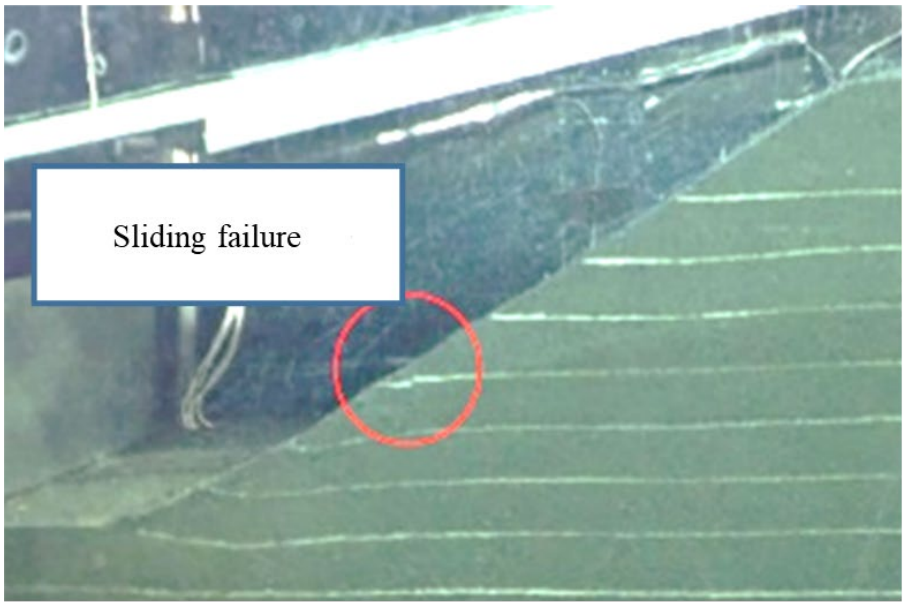

(a)

(b)

Fig. 8. Status of downstream embankment slope after shaking: (a) Case 1 (rainfall, then shaking); (b) Case 2 (shaking only). Red circle in (a) indicates sliding failure.

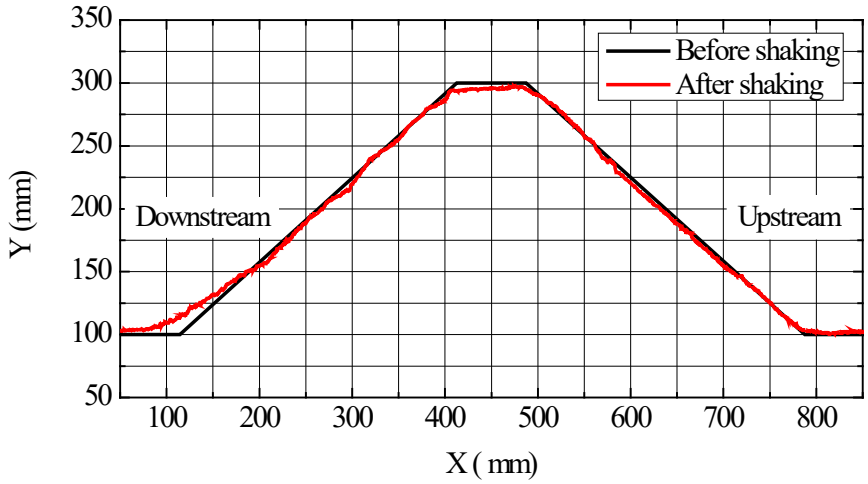

(a)

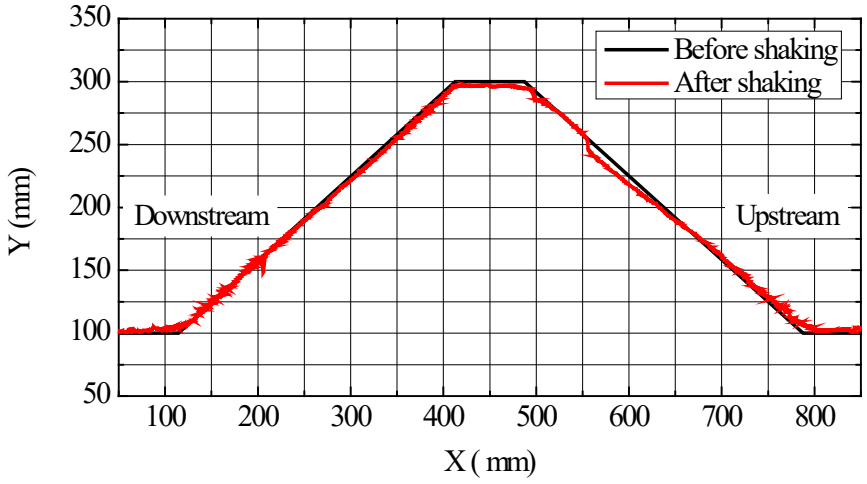

(b)

Fig. 9. Embankment shape after shaking: (a) Case 1 (rainfall, then shaking); (b) Case 2 (shaking only).

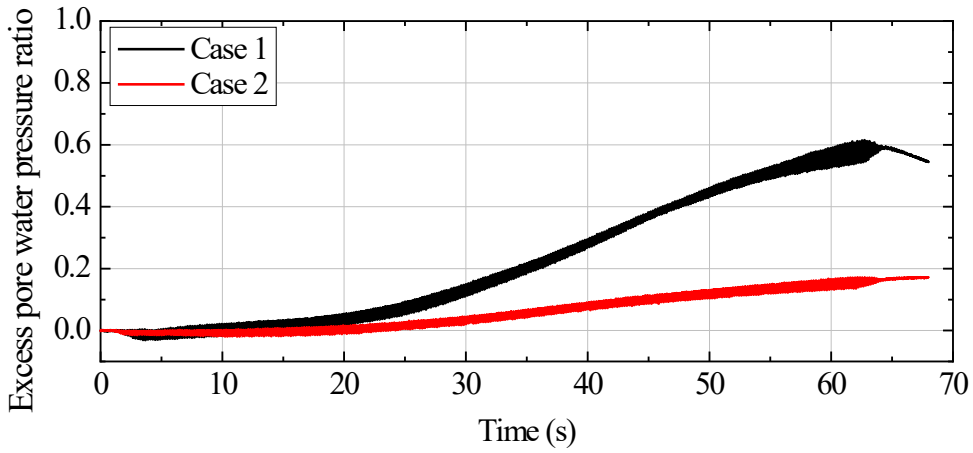

Fig. 10. Excess pore-water-pressure ratio at the toe of the embankment on the downstream side. (Case 1, rainfall, then shaking; Case 2, shaking only.)

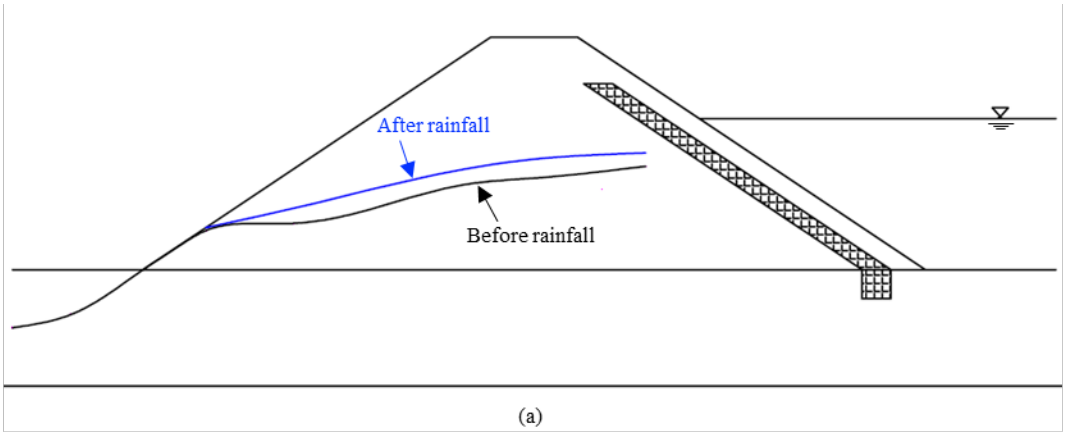

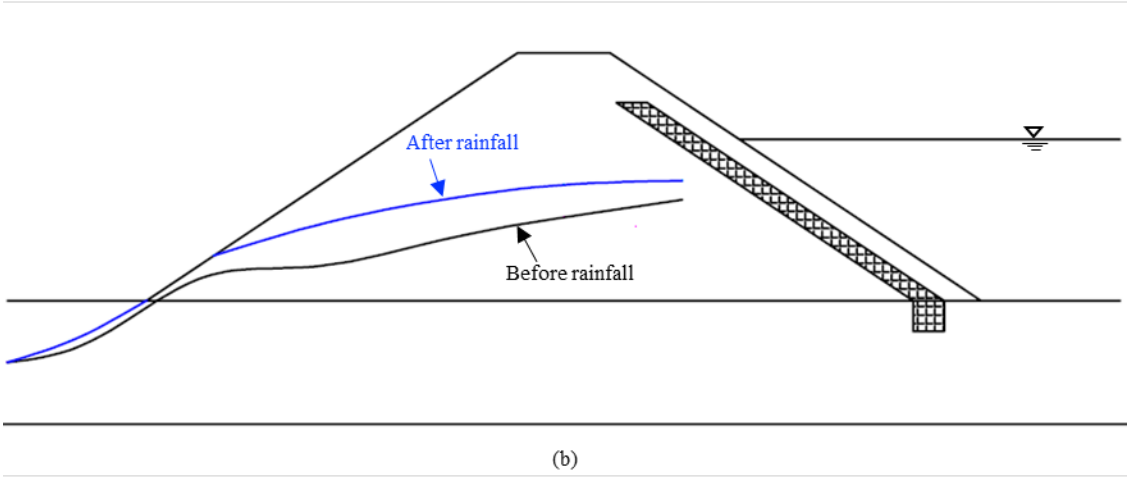

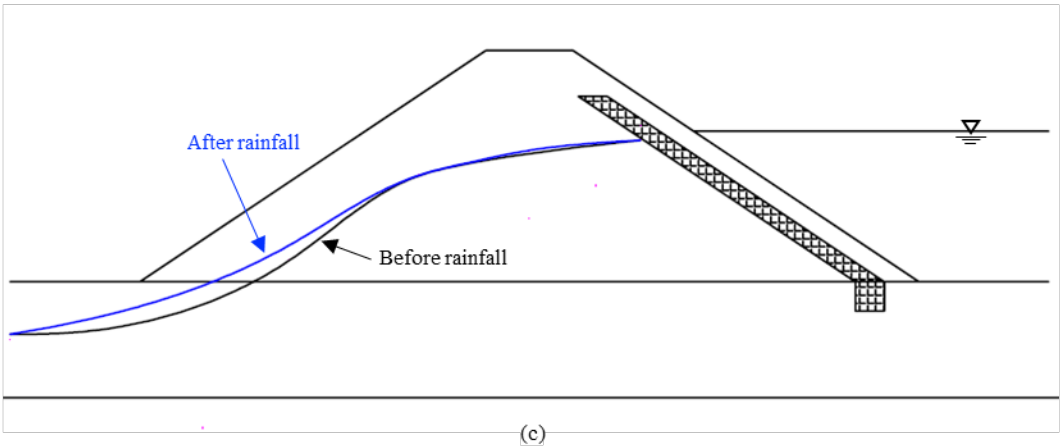

Fig. 11. Phreatic line before and after rainfall: (a) Case 1 (rainfall only); (b) Case 2 (moderate shaking, then rainfall); (c) Case 3 (moderate shaking, then severe shaking, then rainfall).

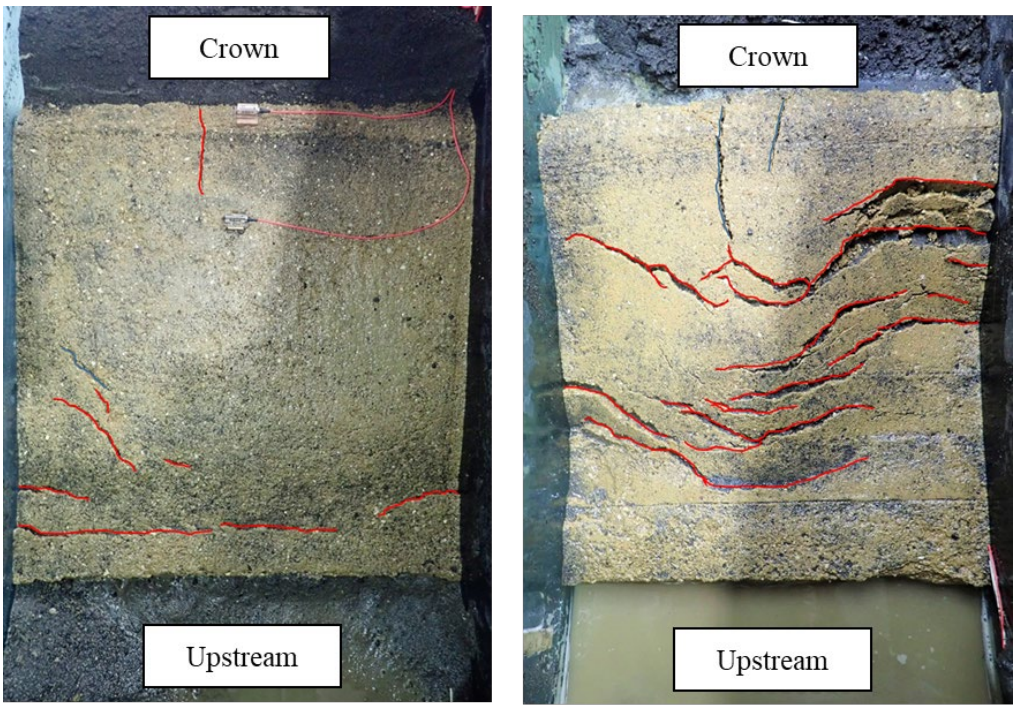

Fig. 12. Status of water-shielding zone (sloping core) after tests: (a) Case 2 (one shaking); (b) Case 3 (two increasingly severe shakings).

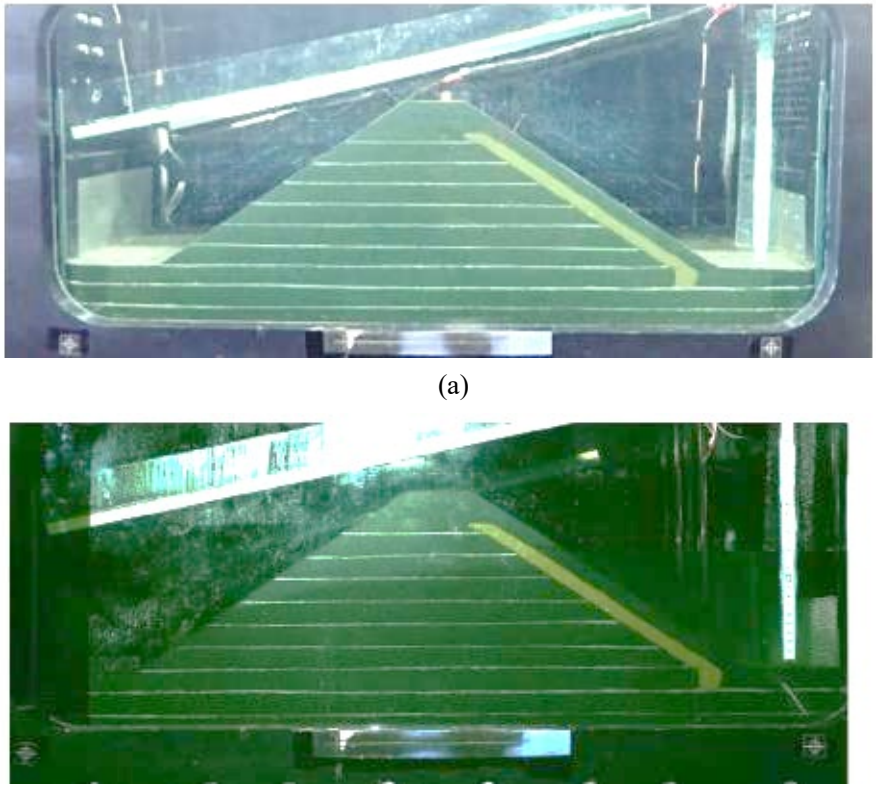

(a)

(b)

Fig. 13. Embankment status (a) before and (b) after rainfall in Case 1 (rain, then shaking). There was almost no deformation.

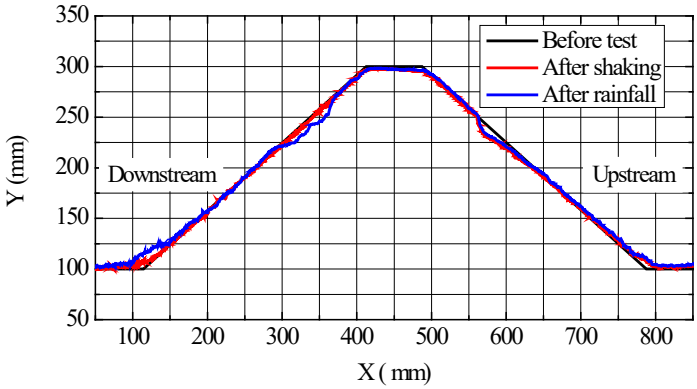

(a)

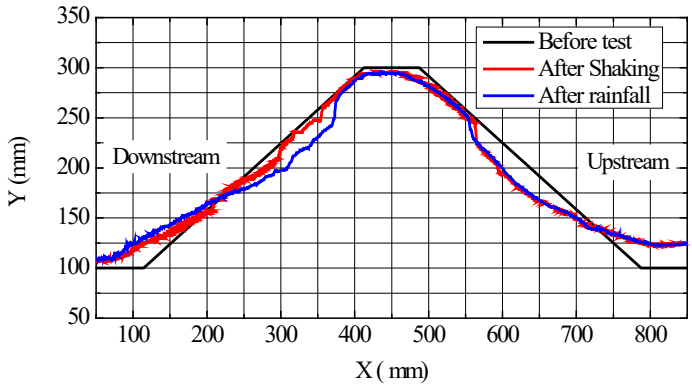

(b)

Fig. 14. Embankment status after completion of tests in (a) Case 2 (one shaking, then rain) and (b) Case 3 (two increasingly severe shakings, then rain). Although rainfall does not normally deform an undamaged embankment, it causes erosion when rainfall seepage occurs in cracks generated by shaking.

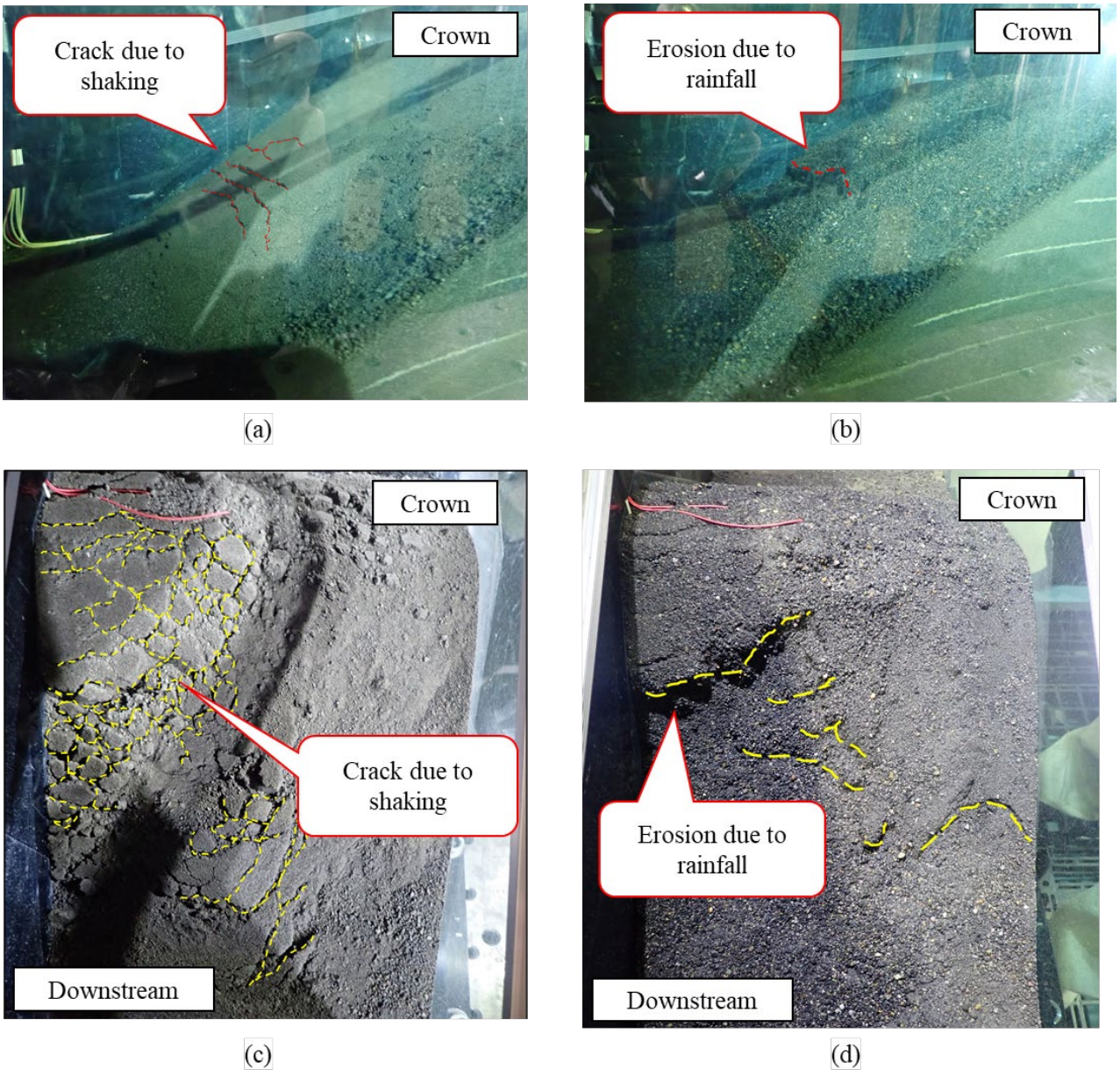

Fig. 15. Status of damage to downstream-slope surface after (left) shaking and (right) rainfall in (top) Case 2 (one shaking before rain) and (bottom) Case 3 (two shakings before rain).

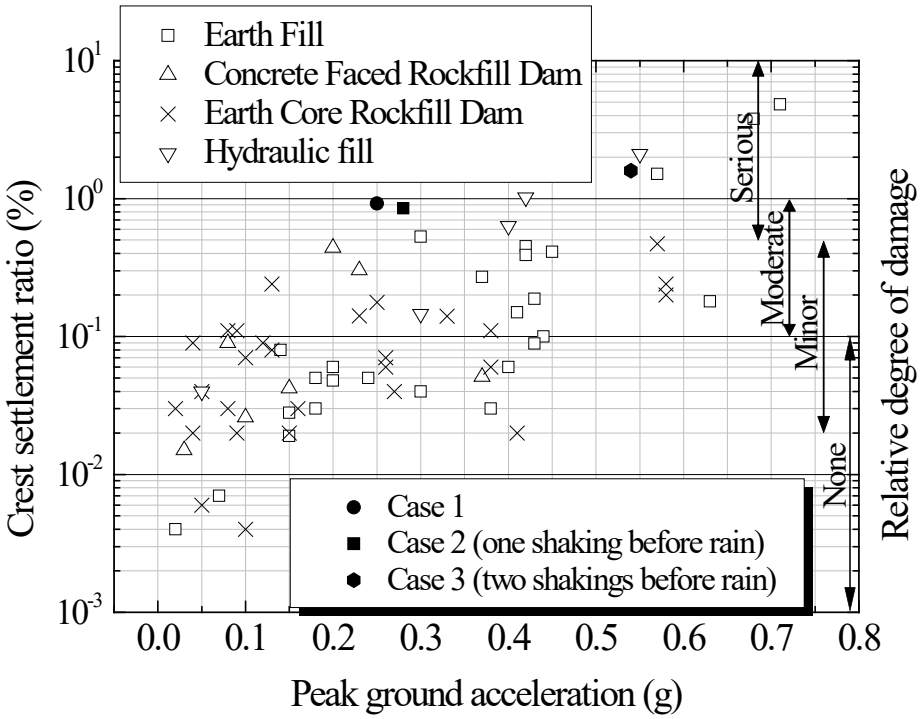

Fig. 16 Relations between peak ground accelerations and crest settlement ratios (modified from Swaisgood, 2003).